Microstructure Development and Crystallization of Poly(ethylene oxide) and Melt-Miscible PEO Blends

Sapna Talibuddin[†] and James Runt*

Department of Materials Science & Engineering, The Pennsylvania State University, University Park, Pennsylvania 16802

Li-Zhi Liu and Benjamin Chu

Department of Chemistry, The State University of New York at Stony Brook, Stony Brook, New York 11794-3400

Received August 21, 1997; Revised Manuscript Received December 11, 1997

ABSTRACT: Time-resolved (TR) small-angle X-ray (SAXS) experiments were conducted to monitor the development of microstructure and crystallinity in neat PEO and a representative composition from four, melt-miscible PEO blends. Although crystal thickening was not observed directly during the time scale of the experiments, comparison of the microstructural parameters obtained from the analysis of the TRSAXS data with those determined from static SAXS (for well-crystallized samples) indicated different rates of crystal thickening for rapidly vs slowly crystallizing systems. An Avrami-like expression was used to track the kinetic evolution of experimental invariants during crystallization. A generalized four-parameter model was proposed which, in addition to the two "Avrami" exponents, included factors that account for the nonzero crystallinity at the start of the SAXS run and finite lamellar stacks at the end of the run. The model is reduced to three parameters for zero initial crystallinity. The three-parameter version could be used successfully to fit the TRSAXS data of the blends (which do not exhibit initial crystallinity), while the four-parameter approach offered a better fit for neat PEO crystallized at 45 °C. The model was further used to estimate bulk crystallinities as a function of time for neat PEO and the strongly interacting blends. These values agree favorably with those measured using DSC.

1. Introduction

Previously, we have used small-angle X-ray scattering measurements and optical microscopy to investigate the influence of diluent mobility, spherulitic growth rate, and strong intermolecular interactions on the microstructure of melt-miscible poly(ethylene oxide) (PEO) blends.[1,2] In the most recent publication,[1] the segregation of weakly interacting polymeric diluents at crystallization temperatures (T_c) of 45 and 50 °C was found to be determined by diluent mobility: relatively high T_g poly(methyl methacrylate) (PMMA) was completely included between PEO lamellae (i.e., resided in interlamellar regions), while lower T_g poly(vinyl acetate) (PVAc) was found to reside partially in interfibrillar regions. In contrast, blends with two strongly interacting copolymers exhibited the same extent of segregation at $T_c = 45$ °C, regardless of diluent mobility. Relatively low T_g ethylene−methacrylic acid (EMAA) and high T_g styrene−hydroxystyrene (SHS) copolymers were preferentially excluded into interfibrillar regions as diluent content was increased to 20%, and became partially interspherultic at higher concentrations. Similar segregation behavior was observed in PEO/SHS blends at $T_c = 50$ °C.[3] Thus the strongly interacting SHS displayed significant diffusion from the crystal growth front whereas its weakly interacting counterpart, PMMA, was trapped within interlamellar regions. Although both low T_g diluents were partially excluded from interlamellar regions, strongly interacting EMAA exhibited larger length scales of segregation.

The average lamellar thickness was found to increase significantly with increasing diluent content for both strongly interacting PEO blends, indicating reduced equilibrium melting points. By comparison of reported values of neat PEO crystal thicknesses at different supercoolings[4] with those of the blends, the melting point depression was estimated to be ∼10 °C for PEO/EMAA and ∼5 °C for PEO/SHS blends containing 20% diluent.[1] In accordance with the depressed degrees of supercooling, severe reductions in spherulitic growth rate were observed in the strongly interacting blends, and the morphologies appeared to assume a more hedritic character (characteristic of low supercoolings) as the diluent content increased from 10 to 30%.[3] Growth rates for the strongly interacting blends were much lower (∼1−2 orders of magnitude) than those for the corresponding weakly interacting blends, even at comparable diluent T_gs.[3]

From these observations, it was inferred that the slow spherulitic growth rates provided the strongly interacting diluents with more time to diffuse over larger distances from the growth front, which is consistent with the predictions of Keith and Padden.[5,6] Furthermore, the presence of strong intermolecular interactions was found to *promote* diluent segregation over greater length scales by depressing the equilibrium melting point (T_m^0) and consequently reducing the growth rate. Accordingly, it was concluded that the diluent segregation is predominately influenced by the spherulitic growth rate for the PEO blends investigated. The segregation behavior of EMAA and SHS further implies that like weakly interacting species, strongly interacting diluents also prefer exclusion from the crystalline microstructure.

In the previous work we focused on the microstructural analysis of well-crystallized PEO and PEO blends.

* To whom correspondence should be addressed.
[†] Present address: General Electric Co., Schenectady, NY.

S0024-9297(97)01265-5 CCC: $15.00
Published on Web 02/18/1998

In the current paper we present the results of an initial synchrotron small-angle X-ray (SAXS) study of the development of microstructure and crystallinity during the crystallization of PEO and selected PEO blends. All samples were analyzed for a period of time well beyond that required for spherulite impingement but shorter than the corresponding times for the well-crystallized samples. Thus, by comparison of the microstructural parameters obtained through the analysis of time-resolved SAXS (TRSAXS) data with those determined for well-crystallized samples ("static" SAXS), the extent of crystal thickening could be investigated. In addition, an Avrami-like model was employed to estimate *bulk* crystallinities (ϕ_c) as a function of time from the TR-SAXS data. As such, bulk crystallinities were calculated for neat PEO and the strongly interacting blends. Similar computations could not be performed for the weakly interacting blends since these calculations require linear crystallinity values which are extracted from analysis of the SAXS correlation function; however, the low electron density contrast in the weakly interacting blends does not permit such analysis. In the case of the PEO/EMAA and PEO/SHS blends, which crystallized relatively slowly, $\phi_c(t)$ were additionally measured by differential scanning calorimetry (DSC) and compared with corresponding values from TRSAXS.

2. Experimental Section

Materials. The polymers used in this study were identical to those used in our previous work.[1,2] PEO of viscosity-average molecular weight 1.44×10^5 was purchased from Polysciences. The two weakly interacting polymers, PMMA and PVAc, were purchased from Aldrich and had T_gs of 113 °C and 31 °C, respectively. $(\bar{M}_w) = 6.4 \times 10^4$, $(\bar{M}_w)/(\bar{M}_n) = 4.4$ for PMMA and $(\bar{M}_w) = 1.3 \times 10^5$, $(\bar{M}_w)/(\bar{M}_n) = 3.1$ for PVAc. The two strongly interacting copolymers, EMAA and SHS, were supplied, respectively, by duPont[7] and Hoechst Celanese. The EMAA copolymer contained 55 wt % methacrylic acid units while SHS consisted of 50 wt % styrene and p-hydroxystyrene. $(\bar{M}_w) = 2.56 \times 10^4$, $(\bar{M}_w)/(\bar{M}_n) = 2.6$ for EMAA and $(\bar{M}_w) = 9.95 \times 10^4$, $(\bar{M}_w)/(\bar{M}_n) = 2.8$ for SHS. Average molecular weights for the amorphous polymers are the polystyrene-equivalent values as determined by gel permeation chromatography.

Bulk crystallinities as a function of time were measured using a Perkin-Elmer DSC 7 differential scanning calorimeter using a perfect heat of fusion of 203 J/g for PEO.[8]

Sample Preparation. Blends were prepared by casting from 2 wt % solutions in a suitable solvent: $CHCl_3$ for PEO/PMMA and PEO/PVAc and 50/50 THF/CH_2Cl_2 for PEO/EMAA and PEO/SHS. The resulting films were dried in air at room temperature for 48 h and then under vacuum at 90 °C for 6 h to ensure complete solvent removal. The dried films were pressed in a Carver hydraulic press at 69 MPa and 100 °C for 2 min and then rapidly cooled in air to room temperature. Neat PEO films were prepared by melt-pressing the powdery polymer under similar conditions. Films were then cut into thin strips and compression molded into 2 mm × 26 mm disks at 69 MPa and 100 °C.

Small-Angle X-ray Scattering. Synchrotron SAXS measurements were performed using a modified Kratky block collimation system on the State University of New York X3A2 Beamline at the National Synchrotron Light Source facility at Brookhaven National Laboratories. Although this camera design utilizes slit collimation, the narrow slit opening (~1.5 mm) results in negligble smearing (~1.5 × 0.5 mm^2 beam cross section at the sample) within the scattering range of interest,[9] i.e., 1 nm$^{-1} \geq q \geq 0.03$ nm^{-1}. q is the scattering vector whose magnitude is defined as $(4\pi/\lambda)\sin(\theta/2)$, with θ being the scattering angle and λ the X-ray wavelength. The storage ring was operated at 2.6 GeV and 110−180 mA, and an X-ray wavelength of 0.154 nm was used. The scattered intensity was collected by a linear position sensitive photodiode detector[10] coupled to an optical multichannel analyzer.

Table 1. Experimental Conditions for TRXAXS Experiments

system	T_e (°C)	tot. run time (s)	t_s (s)	t_c (h)
neat PEO	45	400	<60	6
	50	600	~360	24
80/20 PEO/PVAc	45	600	<90	12
80/20 PEO/PMMA	45	600	~120	24
85/15 PEO/EMAA	45	600	~210	48
80/20 PEO/SHS	45	3340	~2160	48

A selected sample from each blend system was crystallized at 45 °C while T_cs of 45 and 50 °C were employed for neat PEO. Details of sample compositions and experimental run times are presented in Table 1. Corresponding spherulite impingement times (determined via optical microscopy and denoted by t_s) and times for which the well-crystallized static SAXS samples were crystallized isothermally (t_c) are also provided. t_c is very much in excess of the time for complete crystallization at a given T_c. Samples were heated to 100 °C, then quickly transferred to a chamber held at T_c. Data were acquired at 20 s intervals, except in the case of the PEO/SHS blend for which time intervals ranging from 20 to 300 s were used. Since each sample took approximately 20 s to equilibrate at T_c, the first data were collected after an initial 20 s delay.

For each sample, background scatter (from air and instrumentation) was collected before running the sample and subtracted from the experimental data. Corrections for detector nonuniformity were not deemed necessary as the detector pixel sensitivity was nearly linear in the channel range used to collect the data. Intensity fluctuation corrections were made by normalizing the experimental intensities of a set of sample runs with the value of the incident beam intensity recorded just prior to running the sample. For each sample, sample absorption corrections were performed as follows. Any features and spikes, if present, were removed from the first dynamic run. The resulting trace was treated as a "baseline" intensity spectrum and subtracted from all of the dynamic runs, including the first. The data were then smoothed to minimize electronic noise in the high q region.

The one-dimensional correlation function was calculated for all dynamic runs[11]

$$G(r) = (^1/_2\pi^2) \int q^2 I(q) \cos(qr)\, dq \qquad (1)$$

where r is the correlation distance. In favorable cases (where the electron density difference between the crystalline and amorphous components is sufficiently large), the crystalline and amorphous layer thicknesses were derived using the procedure detailed in ref 1. For a "pseudo-two-phase" model, the ordinate of the linear fit to the self-correlation portion of the correlation function gives the experimental invariant, Q_{fit}. Q_{fit} is given by

$$Q_{fit} = v_s w_c (1 - w_c) \Delta\eta_l^2 \qquad (2)$$

where w_c is the linear crystallinity (given by the ratio of the average lamellar thickness, l_c, to the average long period, L), v_s represents the volume fraction of lamellar stacks (given by the ratio of the bulk crystallinity, ϕ_c, to the linear crystallinity) and $\Delta\eta_l$ is the linear electron density difference defined as $\Delta\eta_l = \eta_c - \eta_a$, where η_c and η_a are the electron densities of the crystal and amorphous layers, respectively.

3. Results and Discusssion

Development of Microstructure. For each sample, the raw I vs q data were converted to Lorentz-corrected intensities and correlation functions were generated. Typical results are presented in Figure 1. Figure 1a depicts selected Lorentz-corrected intensity plots for neat PEO crystallized at 45 °C, and Figure 1b, presents

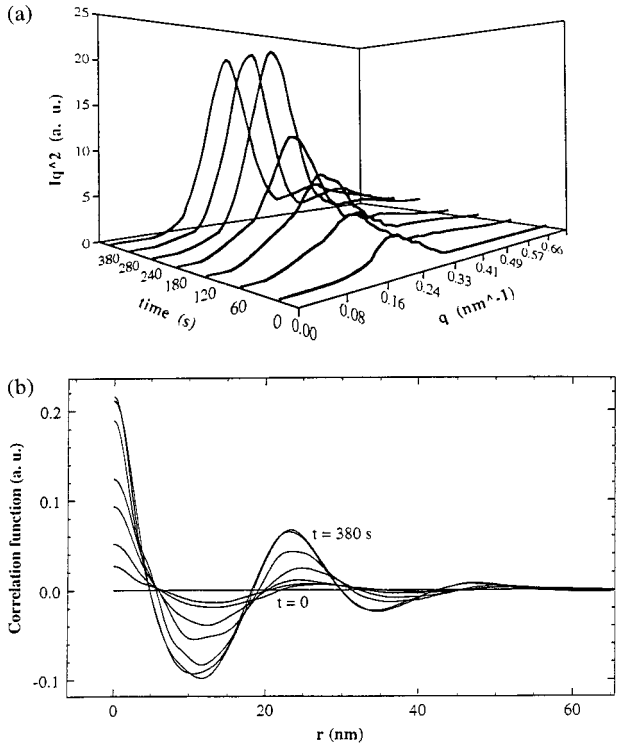

Figure 1. Microstructure development with crystallization time for neat PEO at T_c = 45 °C: (a) Lorentz-corrected intensities vs scattering vector; (b) one-dimensional correlation functions.

the corresponding one-dimensional correlation functions. The Lorentz-corrected intensities progressively increase with time as do the amplitudes of the correlation functions, reaching a more or less constant value at longer times. This behavior is typical of crystallizing polymers[12−14] and can be explained as follows: During crystallization, the volume fraction of lamellar stacks increases as more and more of the amorphous mother phase is depleted and incorporated into the growing spherulites; therefore, the scattering intensity increases with time. As crystallization nears completion, v_s approaches a constant value, which is reflected in the constant Lorentz peak intensity.

Vonk has theoretically shown that finite lamellar stacks reduce the one-dimensional correlation function by a factor that corresponds to the volume fraction of lamellar stacks.[15] This effect has been included in the definition of the invariant in eq 2 and was exploited in ref 1 to determine the fraction and composition of interfibrillar material. An examination of the changes in the general shape of the correlation function with increasing crystallization time is instructive: As crystallization proceeds, the *y*-intercept (related to the invariant) increases, the amplitude of the minimum decreases and that of the first correlation maximum increases. However, the positions of the minimum, first correlation maximum (which gives the average long spacing, henceforth referred to as L_{corr}) and r_0 (intersection of the self-correlation portion of the correlation function with the *x*-axis) remain essentially unaltered by changes in the volume fraction of lamellar stacks. The observation of a correlation maximum and consequently, L_{corr}, requires, first, the formation of lamellar stacks (which may not occur in the very early stages of crystallization[14]) and, second, sufficient quantity of stacks for the maximum to be discernible.

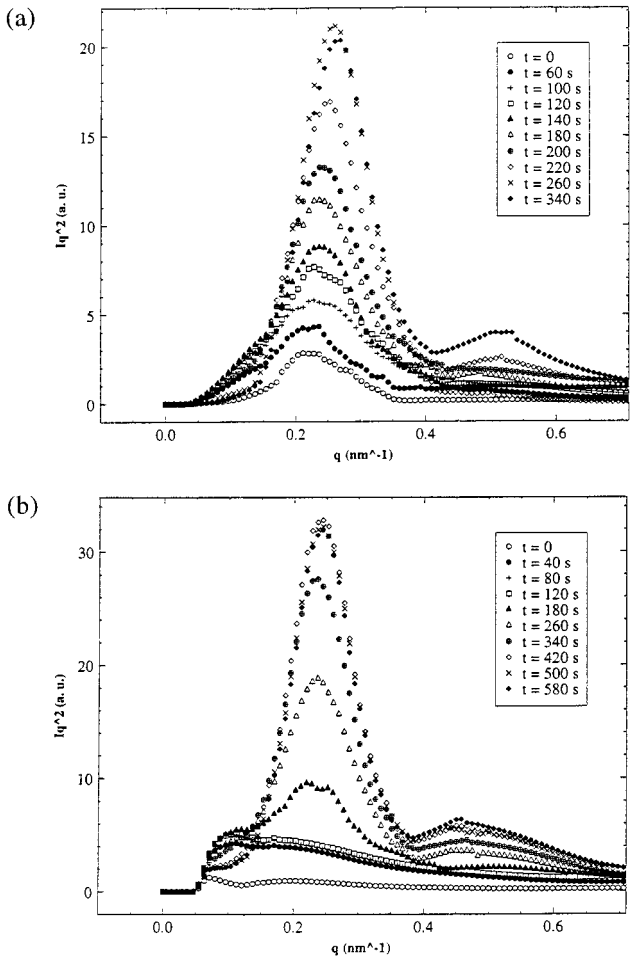

Figure 2. Development of Lorentz-corrected intensities with crystallization time for neat PEO crystallized at (a) 45 °C and (b) 50 °C.

Neat PEO. Figure 2 depicts the development of Lorentz-corrected intensities for neat PEO crystallized at 45 and 50 °C. At both crystallization temperatures, the long periods derived from the Lorentz peak positions appear to decrease initially and then attain constant values that are nearly identical to the corresponding static SAXS long periods determined in ref 1. Similar behavior has been reported for isothermally crystallized poly(ethylene terephthalate)[16] and poly(ether ether ketone).[17] As shown in Figure 2a, at the lower T_c, well-defined peaks were obtained from $t = 0$ and yielded well-defined correlation functions at all time intervals. In contrast, at 50 °C, a distinct peak was not observed until 160 s.

Microstructural parameters extracted from the correlation function analysis are presented in Figure 3 for both T_cs. The corresponding static SAXS values are denoted by solid lines. At 45 °C, the general trend exhibited by L_{corr} is similar to that of the Lorentz long periods. The average lamellar thickness (l_c) remains constant (within experimental error) throughout the duration of the experiment and is in good agreement with the long-term value. Although uncertainties in average amorphous layer thicknesses (l_a) are relatively large, the general trend suggests some thinning of the interlamellar regions at longer times to thicknesses that match up well with the long-term l_a. For T_c = 50 °C, correlation maxima are not observed initially due to the highly damped nature of the correlation functions. For $t \geq 160$ s, L_{corr}, l_c, and l_a appear to exhibit very little

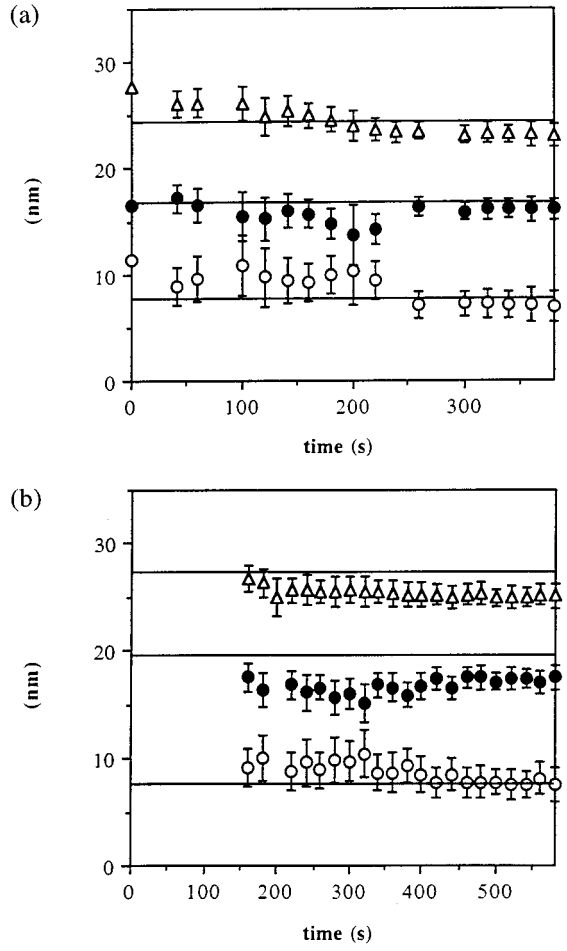

Figure 3. Microstructural parameters vs crystallization time for neat PEO crystallized at (a) 45 °C and (b) 50 °C. Legend: (△) average L_{corr}; (●) average l_c; (○) average l_a. Solid lines denote corresponding parameters determined by static SAXS.

change with time; however, the uncertainties in the calculated values make it difficult to detect any subtle trends. The long periods and lamellar thicknesses seem a little smaller than their long-term values but in light of the ±1 nm uncertainty in the static SAXS L_{corr} and l_c, these can be considered to be comparable, within experimental error.

PEO Blends. Lorentz-corrected intensity plots at selected time intervals are displayed in Figure 4 for the four PEO blends crystallized isothermally at 45 °C. All of the plots exhibit the same general trend, that is, peak intensities increase rapidly at first and then more or less level off at longer times. The long periods for the PEO/PMMA and PEO/EMAA blends (parts b and c of Figure 4, respectively) decrease initially whereas those for PEO/PVAc and PEO/SHS (Figure 4a,d) appear to remain constant with time. As noted previously, correlation functions were not used for microstructural analysis in the case of the 80/20 PEO/PVAc and PEO/PMMA blends. As such, microstructural information was only provided by the long periods determined from Lorentz peaks and correlation maxima. These are depicted in Figure 5. Corresponding static SAXS values are represented by solid and broken lines, respectively. With increasing time, the long periods for the PEO/PVAc remain fairly constant and are very similar to the static SAXS value. For the PEO/PMMA blend, however, the Lorentz long periods decrease rapidly from ~32 nm to a constant thickness of ~26 nm, which is approximately 5 nm lower than the corresponding static SAXS long period. L_{corr} values are also ~5 nm below those from static SAXS.

Microstructural parameters obtained from the correlation functions for 85/15 PEO/EMAA and 80/20 PEO/SHS are presented in Figure 6. For both blends, L_{corr}, l_c, and l_a stay fairly constant throughout the experiment (since reliable correlation functions could not be calculated at the beginning of the crystallization process, the initial decrease in L for the PEO/EMAA blend is not reflected in Figure 6a). L_{corr} and l_c are considerably smaller than the corresponding long-term parameters whereas l_a values lie more or less in the vicinity of the static SAXS l_a. Note that in the case of the PEO/EMAA blend, although 16 L_{corr} values are depicted in Figure 6a, l_c and l_a are presented for only eight time intervals since the self-correlation portions for the other eight intervals exhibited high levels of noise.

Crystallization Kinetics. Typical plots of the experimental invariants vs time are presented in Figures 7 and 8. The general shape of the curves is similar to those reported for other polymer systems[12,16,18] and is reminiscent of "Avrami-type" crystallization kinetics that are obtained from traditional dilatometric or DSC experiments. Consequently, $v_s(t)$ was assumed to exhibit an Avrami-like dependence; that is, at any instant, t, during crystallization

$$v_s(t) \approx 1 - \exp(-zt^n) \tag{3}$$

where z and n are treated merely as fit parameters in the present study. This relation essentially states that the amorphous mother phase is depleted exponentially as material (both crystalline and amorphous) is incorporated into the growing lamellar stacks. From the preceding microstructural analysis, it is evident that changes in linear crystallinity, w_c, (due to changes in lamellar thickness and long period) are too small to cause significant changes in the invariant. Furthermore, even if the linear crystallinities were to change significantly, the product $w_c(1 - w_c)$, which constitutes the linear crystallinity contribution to the invariant, would not exhibit much change. While fluctuations in $\Delta\eta_l$ are possible during crystallization[16] these too will be insignificant in comparison to the effect of v_s. Therefore, w_c and $\Delta\eta_l$ can be assumed to be constant with time, i.e., $Q_{fit}(t) \propto v_s(t)$. Normalizing the time dependent invariants by the maximum value obtained during the experimental run (i.e., Q_{max})[12,13] leads to

$$Q^*(t) = Q_{fit}(t)/Q_{max} = k_1[v_s(t)] = k_1[1 - \exp(-zt^n)] \tag{4}$$

where k_1 is a function of w_c, $\Delta\eta_l$ and Q_{max}. k_1, z and n can be determined by fitting this model to the experimental Q^* vs t data (three-parameter fit). Consequently, $v_s(t)$ can be computed and used with $w_c(t)$ values (extracted from analysis of the correlation function) to calculate bulk crystallinities [since $v_s = \phi_c/w_c$].

Implicit in the definition of $v_s(t)$ in eq 4 are the assumptions that the sample is completely amorphous at the start of the experiment, i.e., $Q^*(0) = k_1[v_s(0)] = 0$, and $v_s \rightarrow 1$ as $t \rightarrow \infty$ (i.e., at long times, the lamellar stacks are infinite). The results presented earlier demonstrate that the first assumption does not hold for neat PEO crystallized at 45 °C, which is partially crystalline at $t = 0$, while static SAXS results[1] show the

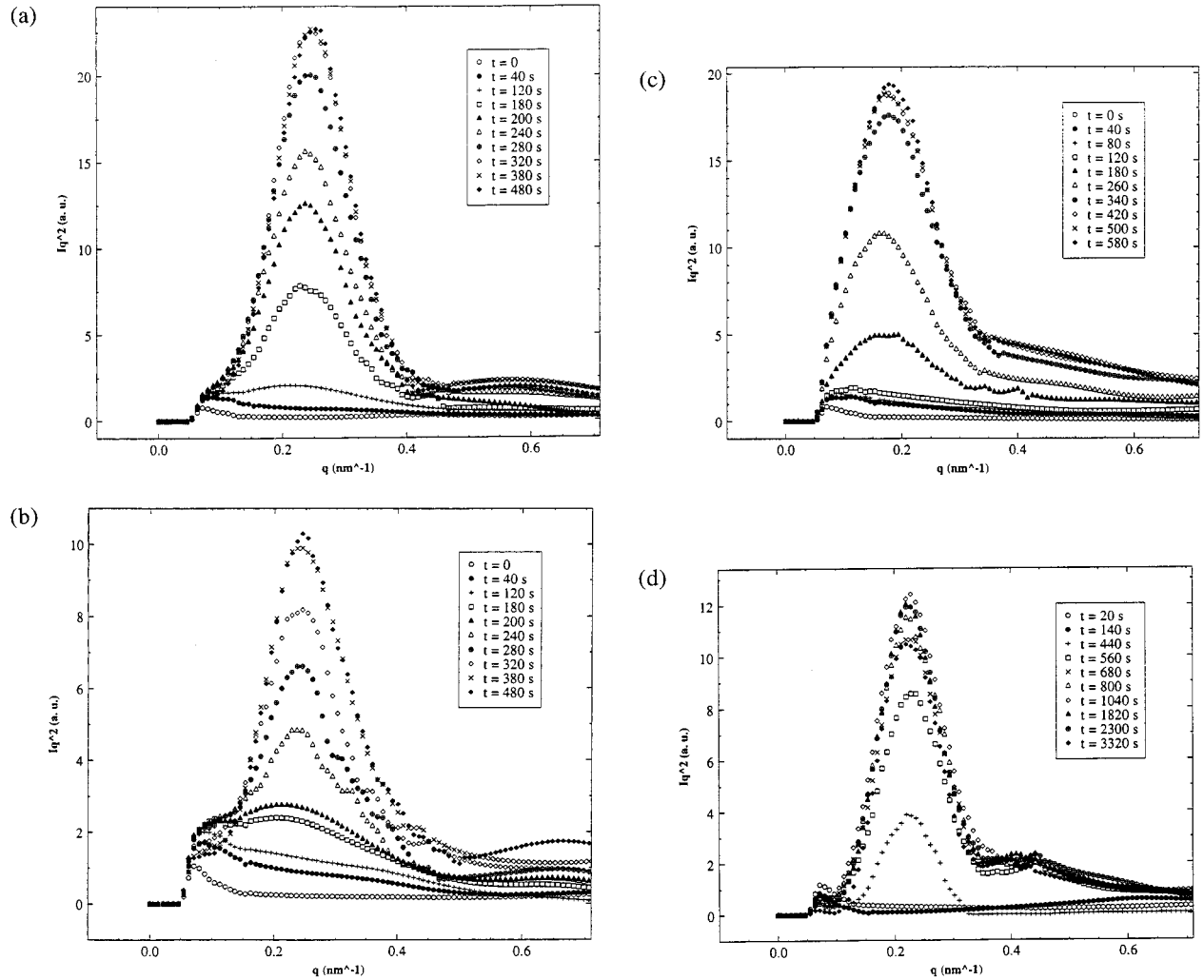

Figure 4. Development of Lorentz-corrected intensities with crystallization time for neat PEO blends crystallized at 45 °C: (a) 80/20 PEO/PVAc; (b) 80/20 PEO/PMMA; (c) 85/15 PEO/EMAA; (d) 80/20 PEO/SHS.

second assumption to be incorrect for the two strongly interacting blends. Thus the definition of $v_s(t)$ is modified as follows:

$$v_s(t) \approx v_{s,stat}[1 - k_2\exp(-zt^n)] \quad (5)$$

Here $v_{s,stat}$ is the long-term volume fraction of lamellar stacks (determined via static SAXS) and k_2 represents the volume fraction of uncrystallized material at $t = 0$. Therefore

$$Q^*(t) = k'[1 - k_2\exp(-zt^n)] \quad (6)$$

where $k' = k_1 v_{s,stat}$. Thus the four-parameter fit (k', k_2, z, and n) provides a more general model for the time dependence of the experimental invariants, whereas the three-parameter model (modified for finite lamellar stacks) presents a special case where $k_2 = 1$.

Q^* vs t plots for neat PEO and the PEO blends are displayed in Figures 7 and 8. As expected, for neat PEO crystallized at 45 °C, eq 6 (solid line in Figure 7a) provides a superior fit to the case where $k_2 = 1$ (broken line) and was used to determine $v_s(t)$. Since PEO crystallized at 50 °C did not form lamellar stacks until 160 s, eq 4 was used to fit the data in Figure 7b. Since $Q^*(0) \approx 0$, the three-parameter approach (but with $k' = k_1 v_{s,stat}$ for the 85/15 PEO/EMAA and 80/20 PEO/SHS blends) was also used to obtain fit parameters for the blends. Model parameters and $v_{s,stat}$ values for neat PEO and the blends are listed in Table 2. For neat PEO crystallized at 45 °C, it appears (from k_2) that approximately 10−20% of the material is crystalline either at the start of or in the initial stages of crystallization. This is consistent with previous optical microscopy experiments.[3]

A realistic comparison of $\phi_c(t)$ estimated from TR-SAXS experiments with those from DSC was not possible for the faster crystallizing systems due to DSC temperature overshoot and the time required for instrument stabilization at T_c. [Recall also that $w_c(t)$ is not available for the weakly interacting blends, and thus $\phi_c(t)$ cannot be calculated]. However, for neat PEO at both crystallization temperatures, linear crystallinities remain fairly constant with crystallization time whereas the calculated $\phi_c(t)$ increases progressively and ultimately levels off to constant values that are in good agreement with the crystallinities determined from the static SAXS samples[1]. At $T_c = 45$ °C, the bulk crystallinities continue to increase after the spherulites have volume-filled, and the overall crystallization time appears to be at least twice as long as that for spherulite impingement. In contrast, at $T_c = 50$ °C, the two times are comparable.

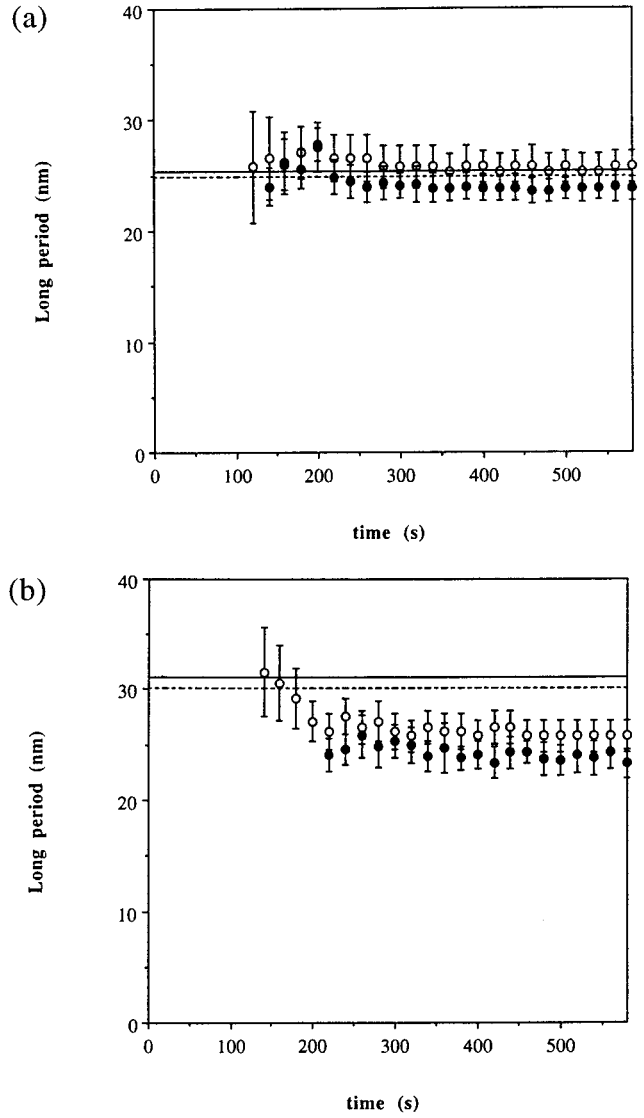

Figure 5. Long periods vs crystallization time for weakly interacting PEO blends crystallized at 45 °C: (a) 80/20 PEO/PVAc; (b) 80/20 PEO/PMMA. Legend: (○) average Lorentz long period; (●) average L_{corr}. Solid and broken lines respectively denote the average Lorentz long periods and L_{corr} determined by static SAXS.

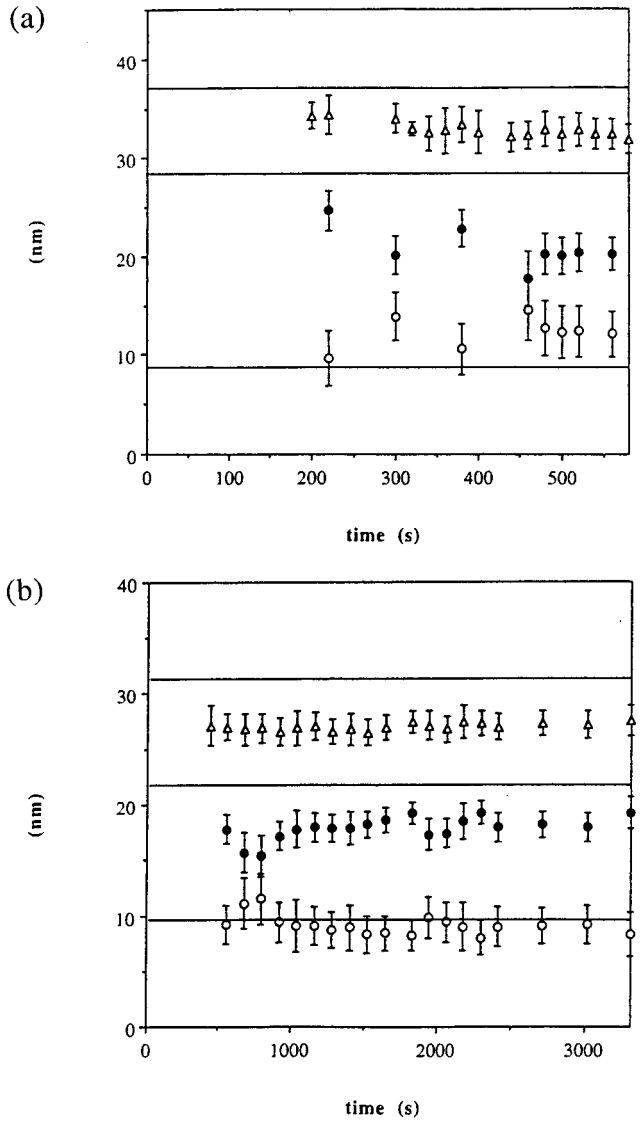

Figure 6. Microstructural parameters vs crystallization time for strongly interacting PEO blends crystallized at 45 °C: (a) 85/15 PEO/EMAA; (b) 80/20 PEO/SHS. Legend: (△) average L_{corr}; (●) average l_c; (○) average l_a. Solid lines denote corresponding parameters determined by static SAXS.

For the 80/20 PEO/SHS blend (Figure 9a), the linear crystallinities also remain constant with time and are similar to that derived from static SAXS. The calculated and DSC bulk crystallinities increase with time at first and then level off. As in the case of the linear crystallinities, the terminal bulk crystallinities (both calculated and measured) are similar to that of the well-crystallized sample. The trends exhibited by the computed and DSC crystallinities are in good agreement, particularly at longer crystallization times. For the PEO/EMAA blend, the DSC bulk crystallinities are larger than the corresponding calculated values. As seen in Figure 9b, the errors in computed bulk crystallinities are rather large, arising primarily from the large standard deviation in the fit parameter, k' (see Table 2). The DSC bulk crystallinities measured toward the end of the run are well below that of the well-crystallized sample used in the static SAXS experiment, implying significant additional crystallization at longer times. For the relatively slower crystallizing PEO/SHS blend, the DSC crystallinities level off at times comparable to the completion of spherulitic crystallization. In contrast, in the case of the PEO/EMAA blend, for which spherulites volume-fill in about 200 s, the DSC crystallinities level off in twice the time, a result which is very similar to that obtained for neat PEO at $T_c = 45$ °C.

Discussion

The results presented earlier for neat PEO crystallized at 45 °C demonstrate that the polymer crystallizes completely during the experimental run, and the lamellae do not appear to thicken during the time frame of the experiment. At $T_c = 50$ °C, the average lamellar thickness and long period are slightly lower than the corresponding static SAXS parameters, perhaps suggesting some limited lamellar thickening at longer times, but the differences are too small to be certain. Except for 80/20 PEO/PVAc, the results for the other PEO blends offer an indication of lamellar thickening at longer crystallization times (i.e., at times longer than the duration of our TRSAXS experiments). Given the relatively short run times and the limited number of specimens, it would be premature to draw sweeping conclusions from the above behavior. It would appear,

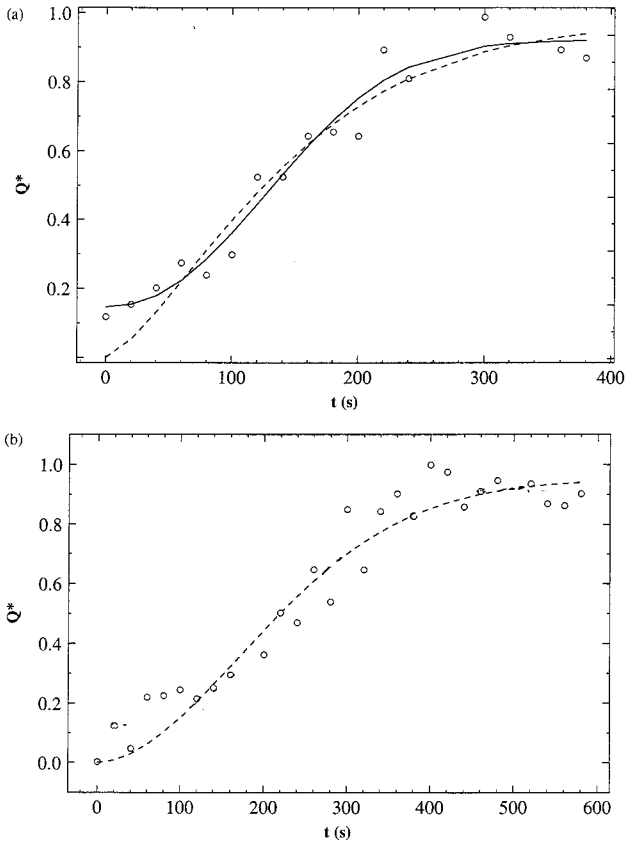

Figure 7. Normalized experimental invariants vs crystallization time for neat PEO at (a) 45 °C and (b) 50 °C. Solid and broken lines in part (a) denote four-parameter and three-parameter fits, respectively. The broken line in part b represents the three-parameter fit.

however, that the rapidly crystallizing systems, such as neat PEO and 80/20 PEO/PVAc, thicken at time scales that are shorter than 20 s (the time intervals at which the data were acquired), or perhaps not at all. In the case of the other three blends, the presence of high T_g and/or strongly interacting diluents presumably slows the thickening process to rates that are too low to detect within the time frame of our experiments, or alternatively, in the case of the strongly interacting blends, the apparent crystalline thickening at longer times may be the result of secondary crystallization in interlamellar and interfibrillar regions, as explained shortly. The initial thinning of the Lorentz long periods observed in neat PEO, 80/20 PEO/PMMA, and 85/15 PEO/EMAA may be due to the insertion of new lamellae in previously existing stacks and real-time melting studies would be helpful in verifying this.

The bulk crystallinities featured in an earlier section invite further scrutiny. Consider the results for neat PEO: At the lower crystallization temperature, the bulk crystallinity continues to increase even after the spherulites have volume-filled, whereas at the higher T_c, ϕ_c levels off at a time that is comparable to the completion of spherulitic growth. The hypothesis put forth previously by Keith and Padden[5,6] can be used to speculate on the origin of the observed behavior. As proposed by the authors, during spherulitic crystallization, less readily crystallizable chains or "impurities" may diffuse adjacent to and/or radially along the fibrils. Since linear growth is observed at both crystallization temperatures, the impurities are expected to preferentially diffuse adjacent to to the lamellar stacks, thus slowing down

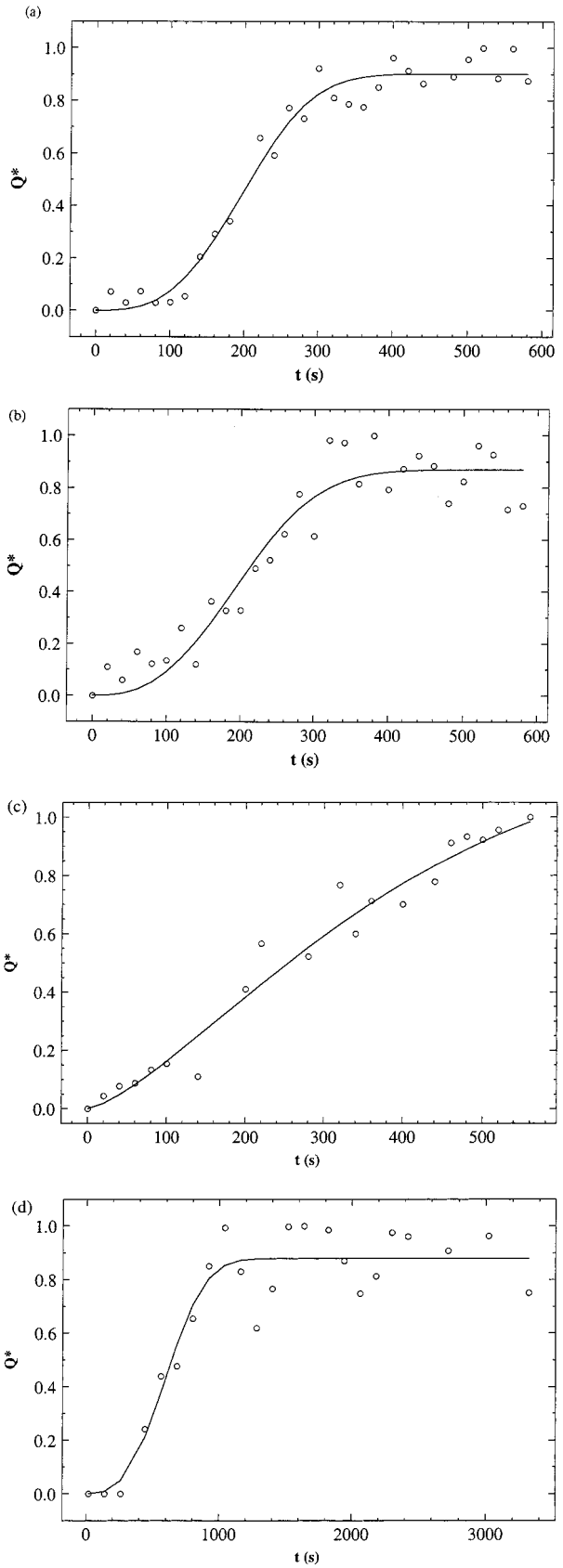

Figure 8. Normalized experimental invariants vs crystallization time for PEO blends at 45 °C: (a) 80/20 PEO/PVAc; (b) 80/20 PEO/PMMA; (c) 85/15 PEO/EMAA; (d) 80/20 PEO/SHS. Solid lines denote three-parameter fits.

crystallization in these regions. At higher supercooling, the rapid growth rate possibly allows only the most readily crystallizable material to crystallize, leading to

Table 2. Model Parameters[a]

system	fit	k'	$v_{s,stat}$	k_1	k_2	z ($\times 10^{-5}$)	n
PEO (T_c = 45 °C)	4-parameter	0.92 ± 0.04	1	0.92 ± 0.04	0.84 ± 0.04	1.07 ± 2.34	2.24 ± 0.42
PEO (T_c = 50 °C)	3-parameter	0.95 ± 0.05	1	0.95 ± 0.05	1	3.30 ± 4.41	1.86 ± 0.25
PEO/PVAc [80/20]	3-parameter	0.90 ± 0.02			1	0.01 ± 0.01	3.07 ± 0.34
PEO/PMMA [80/20]	3-parameter	0.87 ± 0.03	1	0.87 ± 0.03	1	0.05 ± 0.12	2.68 ± 0.47
PEO/EMAA [85/15]	3-parameter	1.27 ± 0.35	0.90 ± 0.04	1.41 ± 0.39	1	24.1 ± 26.4	1.38 ± 0.25
PEO/SHS [80/20]	3-parameter	0.88 ± 0.03	0.78 ± 0.04	1.13 ± 0.07	1	~0.003	2.97 ± 0.79

[a] Model parameters were determined by means of nonlinear least-square fits using PASSAGE graphics and numerics software package. Standard deviations in fitted parameters were computed from the standard deviations of the fits and the corresponding covariance matrices.

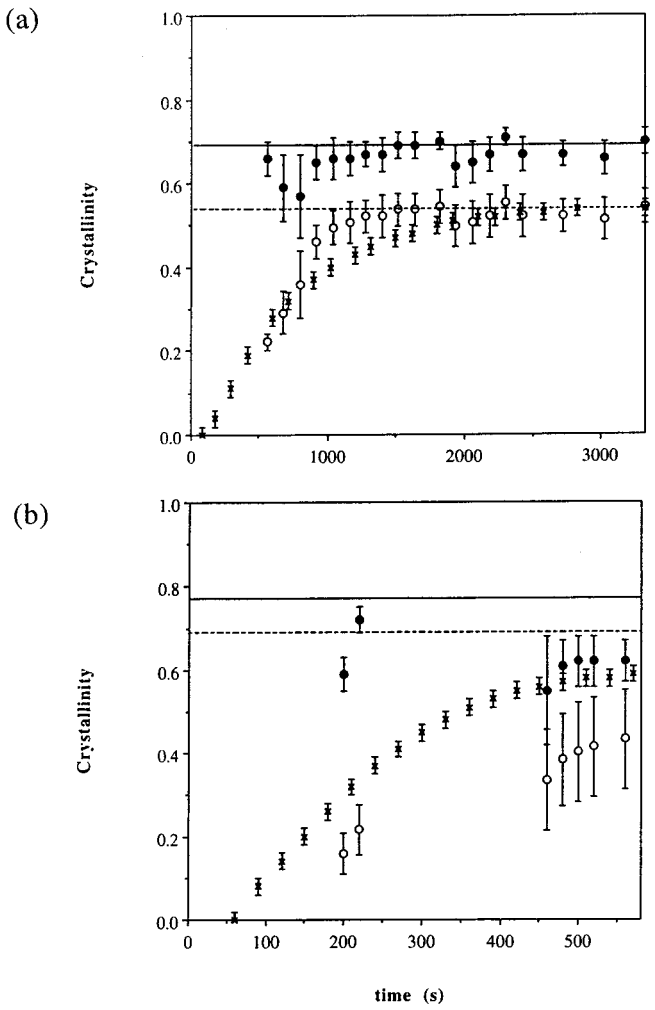

Figure 9. Linear and bulk crystallinities vs crystallization time for strongly interacting PEO blends at T_c = 45 °C: (a) 80/20 PEO/SHS; (b) 85/15 PEO/EMAA. Legend: (●) w_c; (○) computed ϕ_c from TRSAXS; (×) ϕ_c from DSC. Solid and broken lines respectively denote w_c and ϕ_c determined by static SAXS.

a relatively high concentration of slower crystallizing species in the adjacent regions which continue to crystallize even after the spherulites impinge. At the higher crystallization temperature, more chains may order and crystallize, resulting in a much lower impurity concentration in adjacent regions, and consequently, comparable times for spherulite impingement and completion of crystallization.

The same general argument can be extended to overall crystallization vs spherulitic growth observed in 85/15 PEO/EMAA and 80/20 PEO/SHS but this time taking into account the fact that for these blends, the dominant impurities are higher T_g (relative to PEO), strongly interacting diluent polymers. For the PEO/EMAA blend, which exhibits relatively rapid radial spherulitic growth, the above rationale would explain the longer overall crystallization time vs that for spherultic growth. The presence of the strongly interacting diluent in the interfibrillar and interlamellar regions (known from static SAXS experiments) would be expected to further slow the crystallization of PEO in these regions and result in the formation of thicker crystals. This would lead, respectively, to increases in bulk crystallinity and average lamellar thickness at longer crystallization times, as indicated by the difference in crystallinities and l_cs of the static and dynamic SAXS samples. In the case of the PEO/SHS blend, the presence of high T_g SHS in the adjacent regions presumably reduces crystallization in these regions significantly, which would explain the correspondence between the spherulite impingement and overall crystallization times.

Acknowledgment. S.T. and J.R. would like to acknowledge the donors of the Petroleum Research Fund, administered by the American Chemical Society, for their support of this work. B.C. wishes to acknowledge support by the National Science Foundation (DMR9612386) and the SUNY Beamline (DE-FG02-86ER45231).

References and Notes

(1) Talibuddin, S.; Wu, L.; Runt, J.; Lin, J. S. *Macromolecules* **1996**, *29*, 7527.
(2) Barron, C. A. Ph.D. Thesis, The Pennsylvania State University, 1994.
(3) Talibuddin, S. Ph.D. Thesis, The Pennsylvania State University, 1997.
(4) Arlie, J. P.; Spegt, P.; Skoulios, A. *Makromol. Chem.* **1967**, *104*, 212.
(5) Keith, H. D.; Padden, F. J. *J. Appl. Phys.* **1963**, *34*, 2409.
(6) Keith, H. D.; Padden, F. J. *J. Appl. Phys.* **1964**, *35*, 1270.
(7) Lee, J. Y.; Painter, P. C.; Coleman, M. M. *Macromolecules* **1988**, *21*, 346.
(8) Wunderlich, B. *Macromolecular Physics*; Academic Press: New York, 1980; Vol. 3.
(9) Chu, B.: Wu, D.-Q.; Wu. C. *Rev. Sci. Instrum.* **1987**, *58*, 1158.
(10) Chu, B.: Wu, D.-Q.; Howard, R. L. *Rev. Sci. Instrum.* **1989**, *60*, 3224.
(11) Strobl, G. R.; Schneider, M.; Voigt-Martin, I. *J. Polym. Sci., Polym. Phys. Ed.* **1980**, *19*, 1361.
(12) Song, H. H.; Wu, D.-Q.; Chu, B.; Satkowski, M.; Ree, M.; Stein, R. S.; Philips, J. C. *Macromolecules* **1990**, *23*, 2380.
(13) Cheung, Y. W.; Stein, R. S.; Chu, B.; Wu, G. *Macromolecules* **1994**, *27*, 3589.
(14) Albrecht, T.; Strobl, G. *Macromolecules* **1996**, *29*, 783.
(15) Vonk, C. G. *J. Appl. Crystallogr.* **1978**, *11*, 541.
(16) Elsner, G.; Koch, M. H. J.; Bordas, J.; Zachman, H. G.; *Makromol. Chem.* **1981**, *182*, 1263.
(17) Hsiao, B. S.; Gardner, K. H.; Wu, D. A.; Chu, B. *Polymer* **1993**, *34*, 3986.
(18) Jonas, A. M.; Russell, T. P.; Yoon, D. Y. *Macromolecules* **1995**, *28*, 8491.

MA971265+